Topological Phase Transitions and Mobility Edges in Non-Hermitian Quasicrystals

Quan Lin,[1] Tianyu Li,[2,3] Lei Xiao,[1] Kunkun Wang,[1] Wei Yi,[2,3,*] and Peng Xue[1,†]
[1]Beijing Computational Science Research Center, Beijing 100084, China
[2]CAS Key Laboratory of Quantum Information, University of Science and Technology of China, Hefei 230026, China
[3]CAS Center For Excellence in Quantum Information and Quantum Physics, Hefei 230026, China

(Received 19 January 2022; accepted 19 August 2022; published 8 September 2022)

Non-Hermiticity significantly enriches the properties of topological models, leading to exotic features such as the non-Hermitian skin effects and non-Bloch bulk-boundary correspondence that have no counterparts in Hermitian settings. Its impact is particularly illustrating in non-Hermitian quasicrystals where the interplay between non-Hermiticity and quasiperiodicity results in the concurrence of the delocalization-localization transition, the parity-time (PT)-symmetry breaking, and the onset of the non-Hermitian skin effects. Here, we experimentally simulate non-Hermitian quasicrystals using photonic quantum walks. Using dynamic observables, we demonstrate that the system can transit from a delocalized, PT-symmetry broken phase that features non-Hermitian skin effects, to a localized, PT-symmetry unbroken phase with no non-Hermitian skin effects. The measured critical point is consistent with the theoretical prediction through a spectral winding number, confirming the topological origin of the phase transition. More interestingly, we also provide the first experimental evidence for mobility edges which are induced by non-Hermiticity. Our Letter opens the avenue of investigating the interplay of non-Hermiticity, quasiperiodicity, and spectral topology in open quantum systems.

DOI: 10.1103/PhysRevLett.129.113601

Non-Hermiticity arises in open systems and can lead to intriguing properties with no Hermitian counterparts [1–28]. Exotic non-Hermitian phenomena such as the parity-time (PT) symmetry and exceptional points [4–11], the non-Hermitian skin effects [12–25], and the non-Bloch bulk-boundary correspondence [12,13] have attracted much attention. The interest is further stimulated by their experimental observation in open systems [29–35], with potential applications in precision measurements, nonreciprocal quantum device, and topological transport. So far, these experiments either focus on non-Hermitian models with no spatial degrees of freedom, or on lattices with discrete translational symmetry. The properties of non-Hermitian quasicrystals remain largely unexplored experimentally.

In closed quantum systems, quasicrystals play host to a wealth of properties [36–43]. For instance, in the one-dimensional Aubry-André-Harper (AAH) model, a finite strength of quasiperiodicity drives the system from an extended metallic state into an Anderson insulator where the bulk eigenstates become exponentially localized [36–40]. The AAH model can also be mapped to the Hofstadter model, and hence to the integer quantum Hall system, revealing a deeper connection with band topology [44–46]. Variations of the AAH model feature different forms of quasiperiodic disorder, as well as interactions, which can further give rise to more exotic phases such as the many-body localized [47–49] or the critically localized states [50–52]. In a recent series of theoretical studies, it has been shown that specific non-Hermitian variants of the AAH model can feature a topological phase transition characterized by a spectral winding number [7,53–57]. Remarkably, such a critical point is a simultaneous demarcation for the delocalization-localization transition, the PT-symmetry-breaking transition, as well as for the onset of the non-Hermitian skin effects when an open boundary condition (OBC) is imposed [53]. Given the uniqueness of such a multicritical point, the experimental simulation of non-Hermitian quasicrystals and the underlying rich critical physics is desirable.

In this Letter, we experimentally simulate a non-Hermitian, PT-symmetric AAH model using photonic quantum-walk dynamics. Building upon our previous experiments of quantum walks with non-Hermitian skin effects [32,33], we further introduce position- and polarization-dependent phase operators to implement quasiperiodicity. Through dynamic observables such as the Lyapunov exponents [23,58], the dynamic inverse participation ratio (DIPR) [52], and the time-evolved photon counts, we confirm key properties of the phases on either side of the multicritical point, as predicted by the spectral winding number.

More interestingly, the measured DIPR further provides evidence for the presence of a mobility edge in the system. Mobility edge [59–64], a critical energy separating localized and extended excitations, is a key concept for understanding localization. While the original AAH model does not naturally allow mobility edges due to self-duality [37], recent theoretical studies have shown that mobility edges can emerge under the interplay of non-Hermiticity and

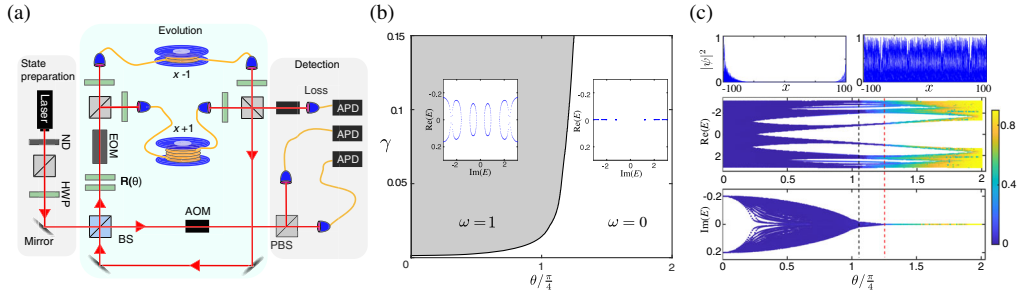

FIG. 1. Simulation of non-Hermitian quasicrystals. (a) A time-multiplexed implementation of the photonic quantum walk. ND: neutral density filter; HWP: half-wave plate; AOM: optical switch acousto-optic modulator; EOM: electro-optic modulator; (P)BS: (polarizing) beam splitter; APD: avalanche photodiode. (b) Phase diagram of the spectral winding number ω. Insets are the typical eigenspectra of the two phases on the complex plane with a fixed $\gamma = 0.1$, and $\theta = \pi/8$ for $\omega = 1$ and $\theta = 3\pi/8$ for $\omega = 0$. The phase boundary here not only marks the onset of the non-Hermitian skin effect, but also the PT-symmetry breaking point and the delocalization-localization transition. (c) Top panel: spatial distribution of all eigenstates of U under the OBC, for the phase with $\omega = 1$ (left) and $\omega = 0$ (right), respectively. Middle panel: the real components of the eigenenergies E of the effective Hamiltonian H (under PBC) with increasing θ, colored according to their respective inverse participation ratio IPR. Lower panel: the imaginary components of the eigenenergies with increasing θ (under PBC), colored according to the IPR. For the numerical simulations, we take the lattice size $N = 200$ and $\gamma = 0.1$. Black and red vertical dashed lines ($\theta/(\pi/4) \approx 1.05$ and $\theta/(\pi/4) \approx 1.25$) indicate the location where a mobility edge emerges and ends in the eigenspectrum, respectively.

quasiperiodic disorder [65,66]. Our experiment constitutes the first experimental observation of non-Hermiticity-induced mobility edges, and offers a valuable quantum mechanical platform for future studies of non-Hermitian quasicrystals.

A time-multiplexed nonunitary quantum walk.—We simulate non-Hermitian quasicrystals using a one-dimensional photonic quantum walk, governed by the Floquet operator

$$U = MSP_2R(\theta)MSP_1R(\theta), \tag{1}$$

where the coin operator

$$R(\theta) = \sum_x |x\rangle\langle x| \otimes \begin{pmatrix} \cos\theta & -\sin\theta \\ \sin\theta & \cos\theta \end{pmatrix},$$

under the polarization basis $\{|H\rangle, |V\rangle\}$, with $|H\rangle$ ($|V\rangle$) the horizontally (vertically) polarized state and x labeling the lattice sites. The shift operator is given by $S = \sum_x |x-1\rangle\langle x| \otimes |H\rangle\langle H| + |x+1\rangle\langle x| \otimes |V\rangle\langle V|$. Non-Hermiticity is introduced through the partial measurement

$$M = \sum_x |x\rangle\langle x| \otimes \begin{pmatrix} e^{\gamma} & 0 \\ 0 & e^{-\gamma} \end{pmatrix}$$

with γ the gain-loss parameter. The position-dependent phase operators satisfy

$$P_1 = P_2^{-1} = \sum_x |x\rangle\langle x| \otimes \begin{pmatrix} e^{\frac{i}{2}\cos(x\pi\phi)\pi} & 0 \\ 0 & e^{-\frac{i}{2}\cos(x\pi\phi)\pi} \end{pmatrix}$$

with $\phi = (\sqrt{5}-1)/2$, the inverse of the golden mean.

For the quantum-walk dynamics, the Floquet operator U repeatedly acts on the initial state $|\Psi(0)\rangle$, with the time-evolved state given by $|\Psi(t)\rangle = U^t|\Psi(0)\rangle$, where t labels the discrete time steps. The quantum walk is therefore a stroboscopic simulation of the time evolution driven by an effective Hamiltonian H, defined as $U = e^{-iH}$ [32,33].

In the absence of the phase operators P_i ($i = 1, 2$), the quantum walk governed by U features non-Hermitian skin effect [32,58]. Therein, the interplay of the effective spin-orbit coupling (the coupling between polarization and spatial modes) and the polarization-dependent loss, leads to a finite, nonreciprocal probability current in the bulk that is responsible for the accumulation of population at boundaries, the namesake phenomenon of non-Hermitian skin effects. The quasiperiodicity is then introduced through the phase operators $P_{1,2}$, which can be understood as a polarization-dependent quasiperiodic potential for the effective Hamiltonian. The resulting Floquet operator U thus realizes a stroboscopic simulation of the dynamics of a generalized non-Hermitian AAH model that features nonreciprocal hopping and quasiperiodic modulation of the on-site potential [67].

As illustrated in Fig. 1(a), we adopt a time-multiplexed scheme for the experimental implementation of U [67]. Pulses from the photon source are attenuated to the single-photon level using a neutral density filter, ensuring a negligible probability of multiphoton events [68,69]. Similar to the setup in Ref. [58], the various operators are implemented using beam splitters and half-wave plates, and are integrated into two optical fiber loops through which each photon passes twice for each discrete time step. Here, different walker positions are encoded into the time domain, thanks to the polarization-dependent time delay introduced through the two optical fiber loops. With these,

the position-dependent phase operators $P_{1,2}$ are realized through an electro-optical modulator that imposes a time-dependent phase within each discrete time step. Finally, we implement a polarization-dependent loss operator $M_E = e^{-\gamma}M$, and the experimentally realized time-evolved state $|\Psi_E(t)\rangle$ is related to $|\Psi(t)\rangle$ through $|\Psi(t)\rangle = e^{2\gamma t}|\Psi_E(t)\rangle$.

Winding number and phase diagram.—The quasicrystalline features of U are best illustrated using the phase diagram characterized by a spectral winding number. To calculate the winding number, we consider a periodic boundary condition (PBC) with N lattices sites, and with an auxiliary magnetic flux Φ threaded through the resulting ring. This is equivalent to making the replacement $\gamma \to \gamma + i\Phi/(2N)$ in U. Subsequently, the spectral winding number is defined as [7,53]

$$\omega = \lim_{N\to\infty} \frac{1}{2\pi i}\int_0^{2\pi} d\Phi \frac{\partial_\Phi \det\{H(\Phi/N) - E\}}{\det\{H(\Phi/N) - E\}}, \quad (2)$$

where H is the effective Hamiltonian of U, and E is a base point in the complex energy plane. The quantum walk has a spectral topology, if there exists an E such that $\omega \neq 0$. In this case, the PBC eigenspectrum of the effective Hamiltonian exhibits closed loops around the base point E, implying a persist current in the bulk which is the origin of the non-Hermitian skin effect under an OBC [20,21]. Otherwise, when $\omega = 0$, the PBC eigenspectrum of H does not have spectral topology, and the quantum walk does not show the non-Hermitian skin effect under OBC. We show in Fig. 1(b), the phase diagram of the system. In the region with $\omega = 1$, the emergence of non-Hermitian skin effect is confirmed in the top panel of Fig. 1(c), where all eigenwave functions accumulate toward the boundaries under OBC.

Under quasiperiodicity, eigenstates of the system undergo a delocalization-localization transition with increasing θ. The localization of the nth eigenstate can be characterized by the inverse participation ratio (IPR) [51] defined as

$$I_n = \sum_x \frac{|\psi_n(x)|^4}{\sum_x |\psi_n(x)|^2}, \quad (3)$$

where $\psi_n(x)$ is the support of the nth eigenstate of U on site x. The state is delocalized (localized) when I_n is vanishingly small (finite). As illustrated in the middle panel of Fig. 1(c), the critical θ appears to be energy dependent across the eigenspectrum, indicating the existence of a mobility edge.

Interestingly, the aforementioned spectral topological phase boundary simultaneously marks the transition point beyond which all eigenstates of the system are localized. In Fig. 1(c), we indicate such a global delocalization-location transition with a dashed vertical line in red. To the right of the line, all I_n are finite, the system is fully localized, and the winding number $\omega = 0$. To the left of the line, not all eigenstates are localized (some states still feature finite I_n), and the winding number $\omega = 1$. One may further identify a transition point [indicated by the black dashed line in Fig. 1(c)] where the first localized eigenstates (the ground and the highest excited states) emerge in the spectrum. This transition marks the onset of the mobility edge as θ increases, but does not coincide with the spectral topological transition.

The spectral topological phase boundary is also the critical point at which the PT symmetry becomes broken under PBC. Because of the spectral topological origin of the non-Hermitian skin effect, the region with $\omega = 1$ is necessarily PT-symmetry broken. Intriguingly, as shown in the lower panel of Fig. 1(c), in the region with $\omega = 0$, the eigenspectrum of H is entirely real, indicating the concurrence of the spectral topological transition, the global delocalization-localization transition, and the PT-symmetry breaking transition [53,67]. In the following, we experimentally probe these transitions one by one.

Non-Hermitian skin effects.—We demonstrate experimentally the mechanism leading to the non-Hermitian skin effect through bulk dynamics [58]. While the direct manifestation of the non-Hermitian skin effect is the accumulation of population at open boundaries, it originates from a persistent, directional bulk current that can be directly probed through bulk dynamics. For this purpose, we initialize the walker near $x = 0$, and record the photon distribution at each time step up to $t = 10$. For $\theta < \theta_c$, the system possesses non-Hermitian skin effects. This is reflected as the directional probability flow in the bulk, as shown in Fig. 2(a). By contrast, for sufficiently large θ, the system is in the Anderson-localized state, and the probability would accumulate at the initial position, as shown in Fig. 2(b).

The conclusion, while consistent with the phase diagram, is further confirmed by measuring the Lyapunov exponent, defined as [23,58]

$$\lambda(v) = \frac{1}{t}\log|(\langle x = vt| \otimes \langle H|)|\Psi(t)\rangle|, \quad (4)$$

where v is the shift velocity. The Lyapunov exponent reveals the presence of the bulk probability flow, since by definition, the location of its peak shows how the wave function propagates along the lattice. Specifically, $\lambda(v)$ peaks at a finite shift velocity v in the presence of non-Hermitian skin effect; whereas it peaks at $v = 0$ in the absence of non-Hermitian skin effect [23,58]. Experimentally, we construct $\lambda(v)$ following a ten-step quantum walk, by measuring the photon distribution at each step. As shown in Figs. 2(c) and 2(d), the experimental data confirm a directional transport in the region with $\omega = 1$. Here, the directional transport is the origin of the non-Hermitian skin effect, as well as its most apparent dynamic signature.

Localization and mobility edge.—To characterize the localization properties, we measure the DIPR [52], defined as $D = \sum_x P^2(x,t)$, where $P(x,t)$ is the corrected probability of the walker on position x at the end of

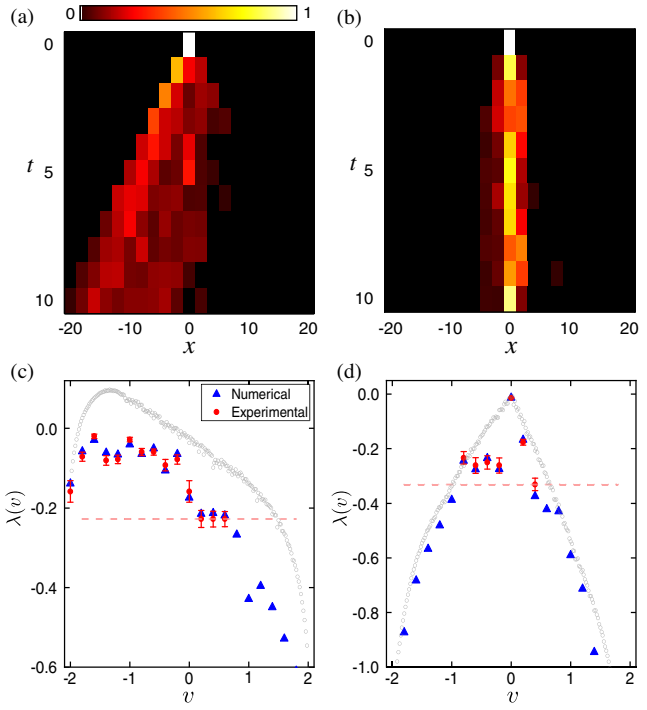

FIG. 2. Dynamic signatures of the non-Hermitian skin effect in a non-Hermitian quasicrystal. Measured photon distributions up to 10 time steps with a fixed $\gamma = 0.1$. The initial state is $|x = 0\rangle \otimes |H\rangle$, and the coin parameters are $\theta = 0.18\pi$ in (a) and $\theta = 0.33\pi$ in (b), respectively. The corresponding numerical results are shown in Supplemental Material [67]. (c),(d) Measured Lyapunov exponent $\lambda(v)$ versus the shift velocity v with the same parameters in (a) and (b). Red dots represent the experimental data, and blue triangles are the corresponding numerical simulations. Gray dotted lines denote the numerical results from 100-step quantum walks. Orange dashed lines indicate the threshold values below which experimental data are no longer reliable due to photon loss. Error bars are due to the statistical uncertainty in photon-number counting. The Lyapunov exponent reveals the presence of the bulk probability flow, since by definition, the location of its peak shows how the wave function propagates along the lattice.

time step t. The probability is normalized by dividing the total photon count after the tth step, so that $P(x,t) = |\langle x|\Psi_E(t)\rangle|^2 / \sum_x |\langle x|\Psi_E(t)\rangle|^2$.

A vanishingly small DIPR at long times suggests the delocalized, metallic phase; while a finite DIPR indicates the onset of localization. As illustrated in Fig. 3(a), the measured DIPR (blue) indicates a transition point near $\theta/(\pi/4) \approx 1.05$, which is consistent with the black vertical dashed line in Fig. 1(c). This is the location where some eigenstates start to be localized, as a mobility edge emerges in the eigenspectrum.

To reveal the global delocalization-localization transition where all eigenstates become Anderson localized, we construct the dynamic normalized inverse participation ratio (DNPR), defined as $D_{\text{norm}} = [2t\sum_x P^2(x,t)]^{-1}$. As shown in Fig. 3(a), the measured DNPR (red) becomes

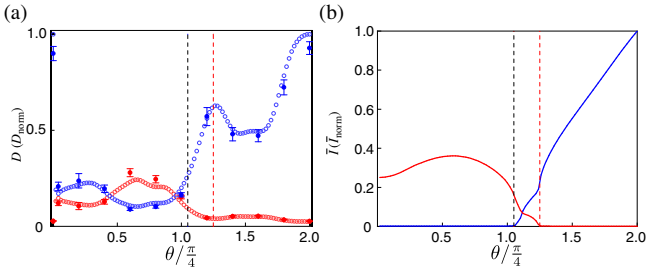

FIG. 3. Observation of the Anderson localization in a non-Hermitian quasicrystal. (a) Measured DIPR (blue) and DNPR (red) for non-Hermitian quantum walks with the initial state $|x = 0\rangle \otimes |V\rangle$. Solid and hollow symbols represent the experimental data and their theoretical predictions, respectively. (b) Numerical simulation of $\bar{I}$ (blue) and $\bar{I}_{\text{norm}}$ (red) for a lattice size $N = 1000$. See the main text for the definitions of $\bar{I}$ and $\bar{I}_{\text{norm}}$. Here, we take $\gamma = 0.1$. Black and red vertical dashed lines indicate the transition points where $\bar{I}$ and $\bar{I}_{\text{norm}}$ are sufficiently small (< 0.02), which are consistent with the definition in Fig. 1(c).

vanishingly small near $\theta/(\pi/4) \approx 1.25$, consistent with the global delocalization-localization transition in Fig. 1(c).

The measured DIPR and DNPR are, respectively, the dynamic probe to the averaged IPR: $\bar{I} = (1/2N)\sum_n I_n$; and the average normalized IPR: $\bar{I}_{\text{norm}} = 1/(4N^2)\sum_n 1/I_n$ [54,70]. Key features in the numerical simulations of these quantities agree well with our measurements [see Fig. 3(b)], indicating a mobility edge in the range $\theta/(\pi/4) \in (1.05, 1.25)$.

Breaking parity-time symmetry.—We confirm the breaking of PT symmetry, by measuring the time evolution of the overall corrected probability of photons. Here, the overall corrected probability is defined as $P(t) = e^{4\gamma t}\sum_x |\langle x|\Psi_E(t)\rangle|^2$, where the exponent $e^{4\gamma t}$ recovers the probability evolution under U. When the system is in the PT

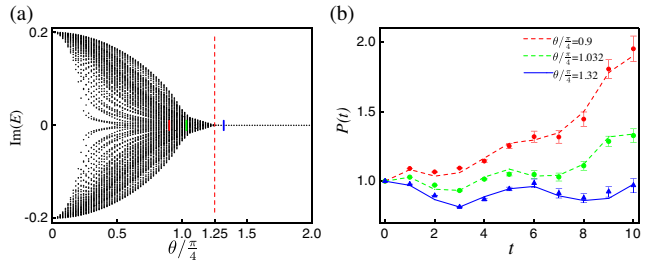

FIG. 4. PT-symmetry transition in a non-Hermitian quasicrystal. (a) Imaginary parts of the quasienergies of a non-Hermitian quantum walk with a lattice size $N = 200$, and $\gamma = 0.1$. The vertical dashed line at $\theta/(\pi/4) \approx 1.25$ separate the PT unbroken and broken phases. (b) Measured overall corrected probabilities $P(t)$ of the quantum walk with an initial state $|x = 0\rangle \otimes |H\rangle$ for various θ corresponding to the PT unbroken and broken phases. Symbols represent the experimental data and curves for their theoretical predictions.

unbroken regime, the quasienergy is entirely real, and $P(t)$ would be on the order of unity. By contrast, when the system is in the PT broken regime, $P(t)$ should grow in time, as the eigenenergies can acquire positive imaginary components. These understandings are confirmed in Fig. 4, where time evolutions at different θ show that the PT transition point is consistent with the theoretical phase diagram.

Conclusion.—We experimentally simulate the dynamics of a one-dimensional non-Hermitian quasicrystal using photonic quantum walks, and reveal a tricritical point where the spectral topological transition, the global delocalization-localization transition, and the PT-symmetry breaking transition simultaneously occur. Our experiment thus unveils a highly nontrivial phenomenon that is absent in Hermitian quasicrystals, and calls for further study of the critical phenomena near these phase transitions.

Intriguingly, the coincidence of all three phase transitions can be model dependent. In a recent theoretical study [40], it is shown that, although the localization and the PT-symmetry breaking transitions coincide in a general class of non-Hermitian quasicrystals, they are not necessarily accompanied by a change of the spectral topology. While the study raises important open questions regarding the conditions for the concurrence of phase transitions, our experiment offers a highly tunable platform on which these questions can be systematically addressed in the future.

This work has been supported by the National Natural Science Foundation of China (Grants No. 12025401, No. U1930402, No. 11974331, and No. 12088101). W. Y. acknowledges support from the National Key Research and Development Program of China (Grants No. 2016YFA0301700 and No. 2017YFA0304100).

Note added.—After the submission of our Letter, a related work [71] appeared, reporting the experimental observation of a topological triple phase transition. In comparison, our implemented model is different, exemplified by the presence of a mobility edge (absent in [71]). This is the first experimental measurement of non-Hermiticity-induced mobility edges based on a quantum-walk configuration.

*wyiz@ustc.edu.cn
†gnep.eux@gmail.com

[1] H. J. Carmichael, Phys. Rev. Lett. **70**, 2273 (1993).
[2] C. M. Bender, Rep. Prog. Phys. **70**, 947 (2007).
[3] R. El-Ganainy, K. G. Makris, M. Khajavikhan, Z. H. Musslimani, S. Rotter, and D. N. Christodoulides, Nat. Phys. **14**, 11 (2018).
[4] C. M. Bender and S. Boettcher, Phys. Rev. Lett. **80**, 5243 (1998).
[5] M.-A. Miri and A. Alù, Science **363**, eaar7709 (2019).
[6] Y. Ashida, Z. Gong, and M. Ueda, Adv. Phys. **69**, 249 (2020).
[7] K. Kawabata, K. Shiozaki, M. Ueda, and M. Sato, Phys. Rev. X **9**, 041015 (2019).
[8] H. Zhou and J. Y. Lee, Phys. Rev. B **99**, 235112 (2019).
[9] A. Ghatak and T. Das, J. Phys. Condens. Matter **31**, 263001 (2019).
[10] J. Li, A. K. Harter, J. Liu, L. de Melo, Y. N. Joglekar, and L. Luo, Nat. Commun. **10**, 1 (2019).
[11] C. Yuce, Phys. Lett. A **378**, 2024 (2014).
[12] S. Yao and Z. Wang, Phys. Rev. Lett. **121**, 086803 (2018).
[13] S. Yao, F. Song, and Z. Wang, Phys. Rev. Lett. **121**, 136802 (2018).
[14] K. Yokomizo and S. Murakami, Phys. Rev. Lett. **123**, 066404 (2019).
[15] C. H. Lee and R. Thomale, Phys. Rev. B **99**, 201103(R) (2019).
[16] F. K. Kunst, E. Edvardsson, J. C. Budich, and E. J. Bergholtz, Phys. Rev. Lett. **121**, 026808 (2018).
[17] D. S. Borgnia, A. J. Kruchkov, and R.-J. Slager, Phys. Rev. Lett. **124**, 056802 (2020).
[18] A. McDonald, T. Pereg-Barnea, and A. A. Clerk, Phys. Rev. X **8**, 041031 (2018).
[19] V. M. Martinez Alvarez, J. E. Barrios Vargas, and L. E. F. Foa Torres, Phys. Rev. B **97**, 121401(R) (2018).
[20] K. Zhang, Z. Yang, and C. Fang, Phys. Rev. Lett. **125**, 126402 (2020).
[21] N. Okuma, K. Kawabata, K. Shiozaki, and M. Sato, Phys. Rev. Lett. **124**, 086801 (2020).
[22] Z. Yang, K. Zhang, C. Fang, and J. Hu, Phys. Rev. Lett. **125**, 226402 (2020).
[23] S. Longhi, Phys. Rev. Research **1**, 023013 (2019).
[24] T.-S. Deng and W. Yi, Phys. Rev. B **100**, 035102 (2019).
[25] L. Li, C. H. Lee, S. Mu, and J. Gong, Nat. Commun. **11**, 5491 (2020).
[26] M. Gräfe, R. Heilmann, R. Keil, T. Eichelkraut, M. Heinrich, S. Nolte, and A. Szameit, New. J. Phys. **15**, 033008 (2013).
[27] S. Scheel and A. Szameit, Europhys. Lett. **122**, 34001 (2018).
[28] T. Jiang, A. Fang, Z.-Q. Zhang, and C. T. Chan, Nanophotonics **10**, 443 (2021).
[29] T. Helbig, T. Hofmann, S. Imhof, M. Abdelghany, T. Kiessling, L. Molenkamp, C. Lee, A. Szameit, M. Greiter, and R. Thomale, Nat. Phys. **16**, 747 (2020).
[30] T. Hofmann, T. Helbig, F. Schindler, N. Salgo, M. Brzezińska, M. Greiter, T. Kiessling, D. Wolf, A. Vollhardt, A. Kabaši, C. H. Lee, A. Bilušić, R. Thomale, and T. Neupert, Phys. Rev. Research **2**, 023265 (2020).
[31] A. Ghatak, M. Brandenbourger, J. van Wezel, and C. Coulais, Proc. Natl. Acad. Sci. U.S.A. **117**, 29561 (2020).
[32] L. Xiao, T. Deng, K. Wang, G. Zhu, Z. Wang, W. Yi, and P. Xue, Nat. Phys. **16**, 761 (2020).
[33] L. Xiao, T. Deng, K. Wang, Z. Wang, W. Yi, and P. Xue, Phys. Rev. Lett. **126**, 230402 (2021).
[34] S. Weidemann, M. Kremer, T. Helbig, T. Hofmann, A. Stegmaier, M. Greiter, R. Thomale, and A. Szameit, Science **368**, 311 (2020).
[35] S. Weimann, M. Kremer, Y. Plotnik, Y. Lumer, S. Nolte, K. G. Makris, M. Segev, M. C. Rechtsman, and A. Szameit, Nat. Mater. **16**, 433 (2017).

[36] P. G. Harper, Proc. Phys. Soc. London Sect. A **68**, 874 (1955).
[37] S. Aubry and G. André, Ann. Isr. Phys. Soc. **3**, 133 (1980).
[38] J. B. Sokoloff, Phys. Rep. **126**, 189 (1984).
[39] S. Longhi, Phys. Rev. B **103**, 054203 (2021).
[40] A. P. Acharya, A. Chakrabarty, D. K. Sahu, and S. Datta, Phys. Rev. B **105**, 014202 (2022).
[41] Y. Lahini, R. Pugatch, F. Pozzi, M. Sorel, R. Morandotti, N. Davidson, and Y. Silberberg, Phys. Rev. Lett. **103**, 013901 (2009).
[42] M. Verbin, O. Zilberberg, Y. E. Kraus, Y. Lahini, and Y. Silberberg, Phys. Rev. Lett. **110**, 076403 (2013).
[43] G. Roati, C. DErrico, L. Fallani, M. Fattori, C. Fort, M. Zaccanti, G. Modugno, M. Modugno, and M. Inguscio, Nature (London) **453**, 895 (2008).
[44] D. R. Hofstadter, Phys. Rev. B **14**, 2239 (1976).
[45] Y. E. Kraus, Y. Lahini, Z. Ringel, M. Verbin, and O. Zilberberg, Phys. Rev. Lett. **109**, 106402 (2012).
[46] L.-J. Lang, X. Cai, and S. Chen, Phys. Rev. Lett. **108**, 220401 (2012).
[47] D. A. Abanin, E. Altman, I. Bloch, and M. Serbyn, Rev. Mod. Phys. **91**, 021001 (2019).
[48] M. Schreiber, S. S. Hodgman, P. Bordia, H. P. Lüschen, M. H. Fischer, R. Vosk, E. Altman, U. Schneider, and I. Bloch, Science **349**, 842 (2015).
[49] M. Rispoli, A. Lukin, R. Schittko, S. Kim, M. E. Tai, J. Léonard, and M. Greiner, Nature (London) **573**, 385 (2019).
[50] J. H. Han, D. J. Thouless, H. Hiramoto, and M. Kohmoto, Phys. Rev. B **50**, 11365 (1994).
[51] Y. Wang, C. Cheng, X.-J. Liu, and D. Yu, Phys. Rev. Lett. **126**, 080602 (2021).
[52] T. Xiao, D. Xie, Z. Dong, T. Chen, W. Yi, and B. Yan, Sci. Bull. **66**, 2175 (2021).
[53] H. Jiang, L.-J. Lang, C. Yang, S.-L. Zhu, and S. Chen, Phys. Rev. B **100**, 054301 (2019).
[54] Y. Liu, Q. Zhou, and S. Chen, Phys. Rev. B **104**, 024201 (2021).
[55] Z. Xu, X. Xia, and S. Chen, Sci. China Phys. Mech. Astron. **65**, 227211 (2022).
[56] Q.-B. Zeng and Y. Xu, Phys. Rev. Research **2**, 033052 (2020).
[57] S. Longhi, Phys. Rev. Lett. **122**, 237601 (2019).
[58] Q. Lin, T. Li, L. Xiao, K. Wang, W. Yi, and P. Xue, Nat. Commun. **13**, 3229 (2022).
[59] P. W. Anderson, Phys. Rev. **109**, 1492 (1958).
[60] P. W. Anderson, Proc. Natl. Acad. Sci. U.S.A. **69**, 1097 (1972).
[61] P. Elyutin, B. Hickey, G. Morgan, and G. Weir, Phys. Status Solidi (b) **124**, 279 (1984).
[62] N. F. Mott, Adv. Phys. **16**, 49 (1967).
[63] N. F. Mott, J. Phys. C **20**, 3075 (1987).
[64] E. Abrahams, P. W. Anderson, D. C. Licciardello, and T. V. Ramakrishnan, Phys. Rev. Lett. **42**, 673 (1979).
[65] Y. Liu, Y. Wang, X.-J. Liu, Q. Zhou, and S. Chen, Phys. Rev. B **103**, 014203 (2021).
[66] Y. Liu, Y. Wang, Z. Zheng, and S. Chen, Phys. Rev. B **103**, 134208 (2021).
[67] See Supplemental Material at http://link.aps.org/supplemental/10.1103/PhysRevLett.129.113601 for details on the experimental methods, detailed characterization of dynamics of the time-evolved state, reality of eigenenergy and localization, dependence of the phase boundary on the gain-loss parameter, as well as additional numerical results.
[68] A. Schreiber, K. N. Cassemiro, V. Potoček, A. Gábris, P. J. Mosley, E. Andersson, I. Jex, and C. Silberhorn, Phys. Rev. Lett. **104**, 050502 (2010).
[69] A. Schreiber, A Gábris, P. P. Rohde, K. Laiho, M. Štefaňák, V Potoček, C. Hamilton, I. Jex, and C. Silberhorn, Science **336**, 55 (2012).
[70] S. Iyer, V. Oganesyan, G. Refael, and D. A. Huse, Phys. Rev. B **87**, 134202 (2013).
[71] S. Weidemann, M. Kremer, S. Longhi, and A. Szameit, Nature (London) **601**, 354 (2022).